IOWA STATE UNIVERSITY
Digital Repository

Retrospective Theses and Dissertations | Iowa State University Capstones, Theses and Dissertations

1-1-2002

Fabrication of giant magnetoresistant devices using electron beam evaporation

David Antonio Garcia
Iowa State University

Follow this and additional works at: https://lib.dr.iastate.edu/rtd

Recommended Citation

Garcia, David Antonio, "Fabrication of giant magnetoresistant devices using electron beam evaporation" (2002). *Retrospective Theses and Dissertations*. 19851.
https://lib.dr.iastate.edu/rtd/19851

This Thesis is brought to you for free and open access by the Iowa State University Capstones, Theses and Dissertations at Iowa State University Digital Repository. It has been accepted for inclusion in Retrospective Theses and Dissertations by an authorized administrator of Iowa State University Digital Repository. For more information, please contact digirep@iastate.edu.

المنارة للاستشارات

www.manaraa.com

Fabrication of giant magnetoresistant devices using electron beam evaporation

by

David Antonio Garcia

A thesis submitted to the graduate faculty

in partial fulfillment of the requirements for the degree of

MASTER OF SCIENCE

Major: Electrical Engineering

Program of Study Committee:
Gary Tuttle, Major Professor
Vikram Dalal
Alan Constant

Iowa State University

Ames, Iowa

2002

للاستشارات المنارة

www.manaraa.com

Graduate College
Iowa State University

This is to certify that the master's thesis of

David Antonio Garcia

has met the thesis requirements of Iowa State University

Signatures have been redacted for privacy

www.manaraa.com

To my wife, Cara Lea, without your
emotional support and superb proofreading skills
this work would not be possible

المنارة للاستشارات

www.manaraa.com

Table of Contents

List of Figures vi

List of Tables vii

Abstract viii

Introduction 1

The Electron 1
Multilayer structures 2
Antiferromagnetic Coupling 4
Different Coercivities 6
Spin-Valves 8
Pseudo Spin-Valves 10
Measuring Techniques 11

Experimental 12

Structure Description 13
Calibration of Evaporator 14
Mixing Metals 15
Evaporation 16
Magnetic Field Generation 17
Fabrication Process 19

Characterization 20

Profilometry 20
Four Point Probe 21
GMR Measurements 22
Bulk Sample 22
Van der Paw 23
Bar Resistors 25
Scanning Electron Microscopy 26
Backscattered electrons 26
Secondary Electrons 27
X-Ray Diffraction 27

Results and Discussion 28

GMR Measurements 30
Hysteresis Measurements 31
Resistivity and Sheet Resistance 34
X-Ray Diffraction 35
Oxygen Incorporation 35
Layer Composition 37
Discussion 37

المنارة للاستشارات
www.manaraa.com

Conclusions **39**
References **41**
Acknowledgements **43**

المنارة للاستشارات
www.manaraa.com

List of Figures

Figure 1 - Electron passing through multilayer GMR stack 3

Figure 2 - Coupling versus thickness of spacer layer 5

Figure 3 - GMR effect versus applied field 6

Figure 4 - Hysteresis loop of a magnetic material 7

Figure 5 - Hysteresis loops of two magnetic materials with different coercivities 7

Figure 6 - Two states for materials with different coercivities 8

Figure 7 - Spin-valve structure 9

Figure 8 - Pseudo spin-valve 10

Figure 9 - CIP and CPP measurement setups 12

Figure 10 - GMR Sandwich Structure 13

Figure 11 - Van der Patterns 24

Figure 12 - Bar resistor 25

Figure 13 - GMR Sandwich Structure 29

Figure 14 -GMR Spin-Valve Structure 30

Figure 15 - Hysteresis plot 1 32

Figure 16 - Hysteresis plot 2 33

Figure 17 - NiFeCo Composition Plot (Powdered Metals) 35

Figure 18 - NiFeCo Composition Plot (Shot Metals) 36

المنارة للاستشارات

www.manaraa.com

List of Tables

Table 1 - Material density and acoustic impedance 16

Table 2 - Fabrication Process 19

Table 3 - GMR Sandwich Structure Growth Parameters 28

Table 4 - GMR Spin-valve Structure Growth Parameters 30

المنارة للاستشارات
www.manaraa.com

Abstract

The discovery of Giant Magnetoresistance (GMR) in 1988 was of great importance to both the research community and industry. The existence of GMR effects has allowed for increase in hard drive storage capacity, and has future potential for use in non-volatile memory and spin-valve transistors. GMR effects are seen in stacks of thin ferromagnetic materials separated by non-magnetic spacer layers. Layer thicknesses are normally on the order of 10 to 50Å.

GMR sandwich structures using Nickel Iron Cobalt (NiFeCo) alloy, Iron Cobalt (FeCo) alloy, Tantalum (Ta), and Copper (Cu) were deposited using Electron Beam (E-beam) Evaporation techniques on Silicon (Si) wafers. A fabrication process was developed to use equipment available at the Microelectronic Research Center. The structures were tested with bulk measurement techniques, Van der Paw patterned measurements, and bar resistor measurements. Films were further characterized using four-point probe resistivity measurements, Scanning Electron Microscopy (SEM), and X-ray diffraction (XRD).

المنارة للاستشارات

www.manaraa.com

Introduction

When giant magnetoresistance (GMR) was first discovered in 1988, its importance was immediately recognized by the research community and industry alike. It has long been known that the path of an electron is altered as it passes through a magnetic field. In metals, changes in electrons' paths cause variations in the resistances. This effect is even more predominant in magnetic materials. The varying effect of the field in relation to the direction of the current flow is also very important. Current flow that is parallel to the applied field will see different variation compared to current flowing perpendicular to the field. This effect is known as magnetoresistance. These magnetoresistant changes vary between different materials from no variation to 5% variation in the most extreme cases.

However, in 1988 Baibich *et al.* [1] and Binasch *et al.* [2] reported magnetoresistive changes on the order of 50% at low temperatures in Iron (Fe)/Chromium (Cr) ultrathin multilayer structures. This phenomenon was inconsistent with the theoretical predictions. These extremely large changes of resistivity were later found to occur in other multilayer structures consisting of alternating magnetic and nonmagnetic materials. The explanation of the GMR effect is due to the characteristics of the electron as it passes through different materials.

The Electron

GMR is a direct result of the unique characteristics of the electron. These tiny negatively charged particles are the current carrying elements in metallic materials. There

المنارة للاستشارات
www.manaraa.com

are three distinctive properties of an electron: a negative charge, a small atomic mass, and the spin. It is the spin of the electron that is the foundation of GMR effects.

As the negatively charged electron spins about itself, it generates a magnetic field. In most materials there are equal numbers of electrons spinning in opposite directions, canceling out their individual moments, resulting in a net magnetic field equal to zero. In a few metals, like Iron (Fe), Nickel (Ni) and Cobalt (Co), the electrons are energetically favored to spin in the same direction. This gives rise to a net magnetic field and a magnetic material.

When a magnetic material is magnetized, the laws of quantum mechanics require that there be only two directions of spin for an electron. An electron is allowed to spin such that its own magnetic field will align with or opposite to the magnetization. When the electron's field is aligned with the magnetization it is said to have 'up' spin. Alternatively, if the electron's field is opposite to the magnetization it has 'down' spin. In a magnetic field most electrons' spins are in the up direction. In nonmagnetic materials, all spins of electrons are expected to respond to magnetic fields in identical ways.

Multilayer structures

The effects of GMR are typically observed in multilayer structures where two magnetic layers are separated by a thin nonmagnetic material. Depending on the relative direction of the magnetization within the magnetic materials, the paths of the up and down electrons will vary. Figure 1 shows a simple depiction of the two possible cases for a simple

المنارة للاستشارات
www.manaraa.com

multilayer structure. The directions of the magnetic fields within the magnetic materials are noted.

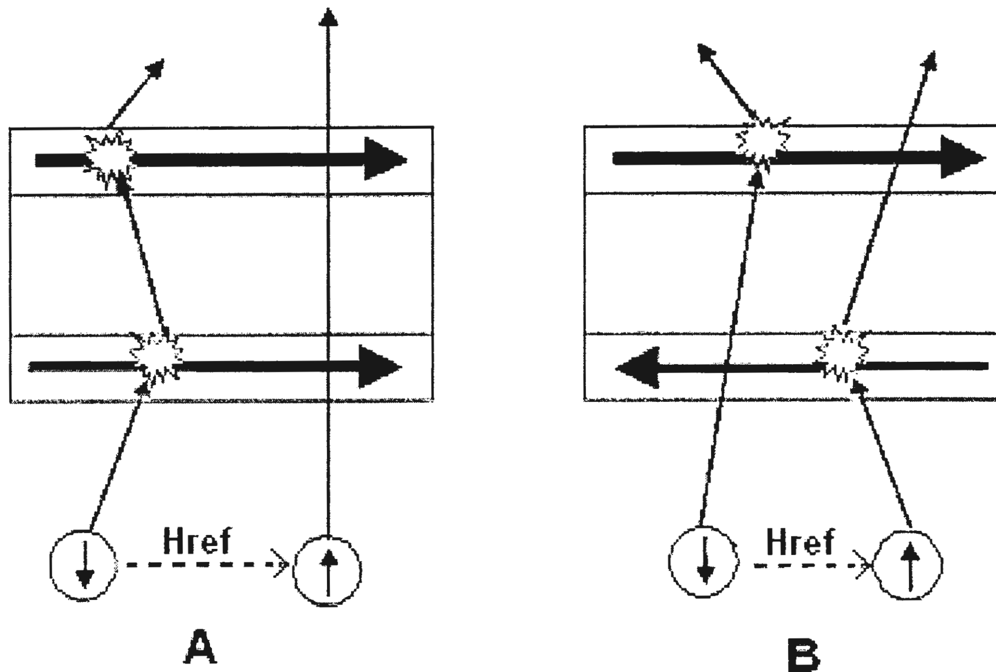

Figure 1 - Electron passing through multilayer GMR stack

If the fields within the two magnetic materials are in the same direction (Figure 1-A), one direction of spin will be able to pass without interference, but the opposite spin will encounter difficulties passing through both magnetic layers. When the fields are opposite (Figure 1-B), electrons of both spin types will experience difficulty as they pass through the structure. While both fields are aligned, the structure has the lowest resistance.

The scattering events that occur in the magnetic materials can more precisely be described in terms of Fermi levels. The band structure of a ferromagnetic material is exchange split, so the density of states for an up electron will be different from that of a

المنارة للاستشارات
www.manaraa.com

down electron. Fermi's law states that the scattering rate is proportional to the density of states. Therefore, the up and down electrons will have different scattering behaviors in the magnetic materials [10].

As a result, two conditions must be met to see GMR effects. First, the thickness of the films used must be less than the mean free path of an electron. Second, there must be a way to independently rotate the magnetizations of the magnetic layers. The first condition can be met by using ultrathin films, keeping individual layers on the order of a few atomic layers. The second condition is more complicated, which has resulted in several different solutions that achieve the desired effect.

Antiferromagnetic Coupling

The magnetic fields of the two magnetic layers can become linked, or coupled, to each other when the layer between them is sufficiently small. The amount that the two layers are coupled is highly dependent on the thickness of this nonmagnetic spacer. Figure 2 shows a plot of the relationship between GMR effects and the spacer layer in a Cobalt (Co)/Copper (Cu) multilayer structure, with the Co layers held constant at 11Å [3].

المنارة للاستشارات
www.manaraa.com

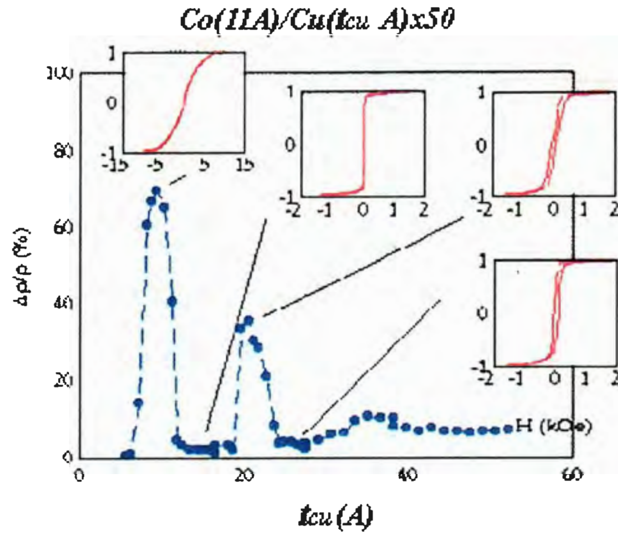

Figure 2 - Coupling versus thickness of spacer layer

The plot in Figure 2 depicts two distinct peeks at approximately 9Å and 21Å, showing the greatest antiferromagnetic coupling factor. As the spacer layer thickness increases, the magnetic layers become uncoupled and do not interact with each other.

Adjacent antiferromagnetically coupled layers are at their lowest energy state when their internal fields lie in opposite directions. For no applied field, the resistance of the multilayer structure will be large. As a magnetic field is applied to the structure the internal fields will rotate so they are in the direction of the applied field, reducing the resistance. At a sufficiently high external field, the structure will be saturated and the resistance will be at a minimum. Figure 3 shows the GMR effects of a Co (11Å)/Cu (9Å) multilayer structure [3].

المنارة للاستشارات
www.manaraa.com

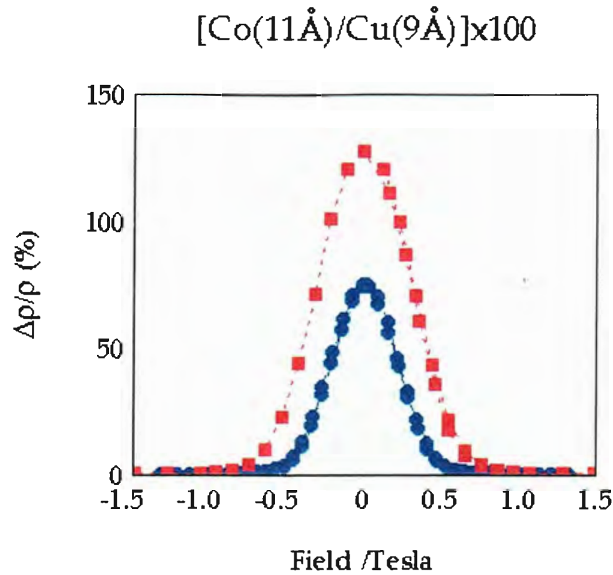

Figure 3 - GMR effect versus applied field

The GMR effects are symmetrical around the zero field point because for any direction of applied field, the internal fields will align. Although this structure does show strong GMR response, a problem arises in the fabrication of a 9Å thick layer of copper. A copper atom is approximately 3Å wide, meaning a three-atom thick layer would be required. It is very difficult to deposit a high quality 9Å film using available deposition techniques.

Different Coercivities

One of the important parameters used in describing the response of a magnetic material to external fields is coercivity. Coercivity (Hc) is defined as the reverse applied magnetic field (H) necessary to reduce the magnetic induction (B) to zero. In relationship to GMR, this is the point where the internal field in the material would switch directions. Figure 4 shows the hysteresis loop (B vs. H) of a magnetic material.

المنارة للاستشارات
www.manaraa.com

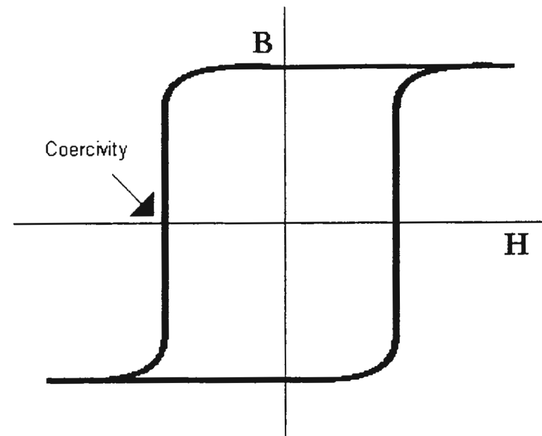

Figure 4 - Hysteresis loop of a magnetic material

By using two magnetic materials with different coercivities, the internal fields of the layers are able to switch directions independently at different applied fields. Hysteresis loops of two different metals each with its own coercivity can be seen in Figure 5.

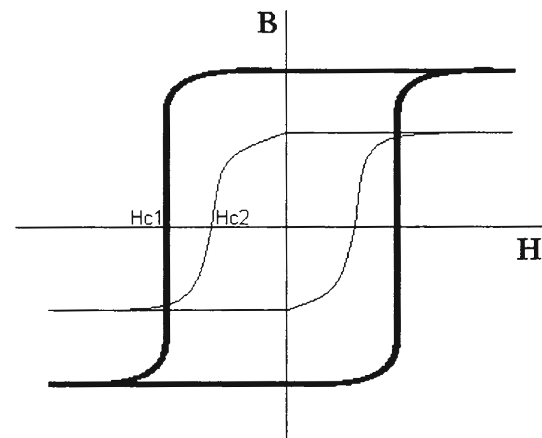

Figure 5 - Hysteresis loops of two magnetic materials with different coercivities

The coercivity of metal 2 is lower than that of metal 1, so the internal field of metal 2 will switch directions at a lower applied field. This is shown graphically in Figure 6. The rotation of the internal fields is symmetrical across the zero applied field.

المنارة للاستشارات
www.manaraa.com

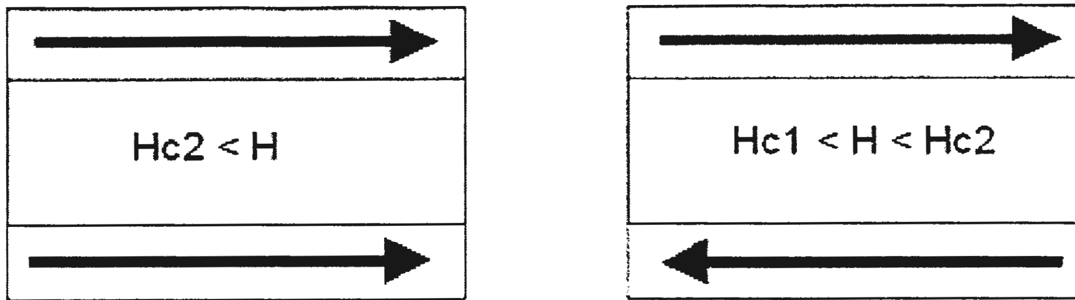

Figure 6 - Two states for materials with different coercivities

Spin-Valves

The spin-valve structure, first proposed by Dieny *et al.* [4], consists of magnetic layers separated by a nonmagnetic spacer layer, thick enough that the magnetic layers are uncoupled. In spin-valves one of the magnetic layers is free to rotate while the other is pinned in one direction. Figure 7 shows the spin-valve structure proposed by Dieny *et al.* [5].

المنارة للاستشارات
www.manaraa.com

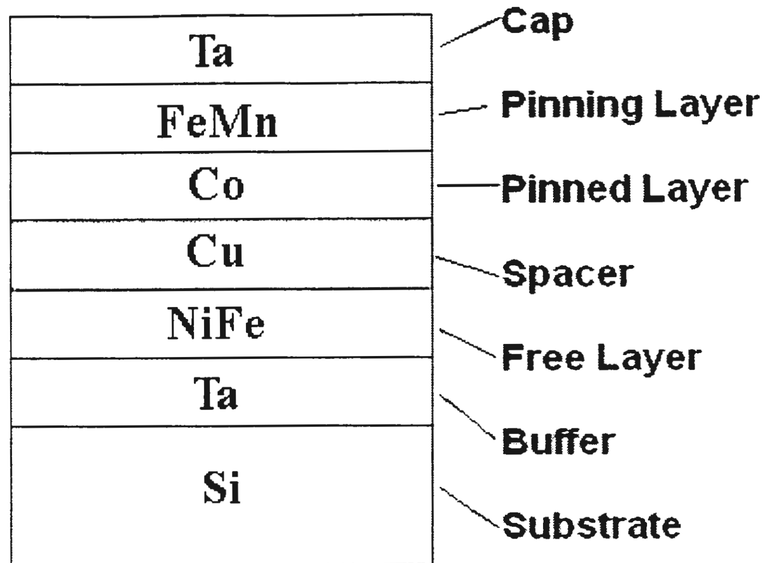

Figure 7 - Spin-valve structure

The Iron-Manganese (FeMn) alloy has a high coercivity, preventing its magnetization from freely rotating in an applied field. The direct contact between the Co and FeMn layers effectively pins the Co layer's internal field in the same direction. This is known as exchange biasing. The soft Nickel-Iron (NiFe) alloy layer is free to rotate with the applied field. Furthermore, the NiFe layer will rotate at much smaller applied fields than needed to rotate the FeMn/Co layers. Because the NiFe layer will rotate at such low fields, this structure is ideal for sensors and other devices used to detect small fluctuations in magnetic fields.

www.manaraa.com

Pseudo Spin-Valves

Pohm *et al.* [11 ,12, 13] proposed the pseudo spin-valve, which uses a similar structure to the spin-valve without a pinned layer. The pseudo spin-valve uses two magnetic layers of the same metal alloy, but differing thicknesses. This difference in thickness results in one of the layers switching direction before the other. In many ways, the pseudo spin-valve structure has similarities to the structure using different coercivities (Figure 6). The pseudo spin-valve structure as outlined by Pohm *et al.* [11, 12, 13] is shown in Figure 8.

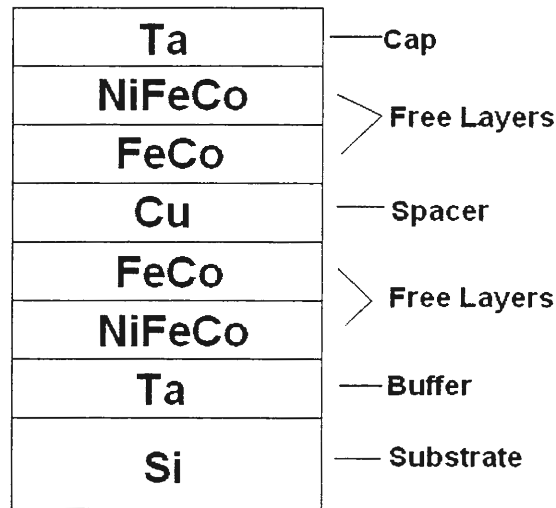

Figure 8 - Pseudo spin-valve

Each free layer in this structure is comprised of two metal alloys, allowing for better film matching at the junctions. The free magnetic layers are uncoupled due to the thickness of the copper spacer layer.

المنارة للاستشارات
www.manaraa.com

Measuring Techniques

There are two predominant techniques used to measure GMR effects, current in the plane (CIP) and current perpendicular to the plane (CPP). CIP uses a four contact configuration on the top layer of the structure. In the CIP measurement, a current is passed from one contact to another, and the induced voltage is measured through the other pair of contacts (Figure 9). With the current held constant, an external magnetic field is applied and the voltage change is monitored. Fluctuations in the voltage can be used to calculate the magnetoresistant changes. This structure gets its name from the current's parallel path along the surface of the film.

CPP uses a pair of contacts on both the top and bottom layers of the structure (Figure 9). The current applied to one of the top contacts will pass through the device, perpendicular to the surface of the films, and out one of the lower contacts. This configuration will still induce a measurable voltage between the remaining upper and lower contacts, which will also change as a field is applied.

Figure 9 shows an illustration of the two types of measurement. CIP is often easier to measure because the setup requires only contacts on the top surface of the device. CPP requires either contacts to be placed before the deposition of the layers or etching following deposition to make contact with the bottom layer. CIP measurements often show lower GMR effects than measurements made using CPP methods.

المنارة للاستشارات
www.manaraa.com

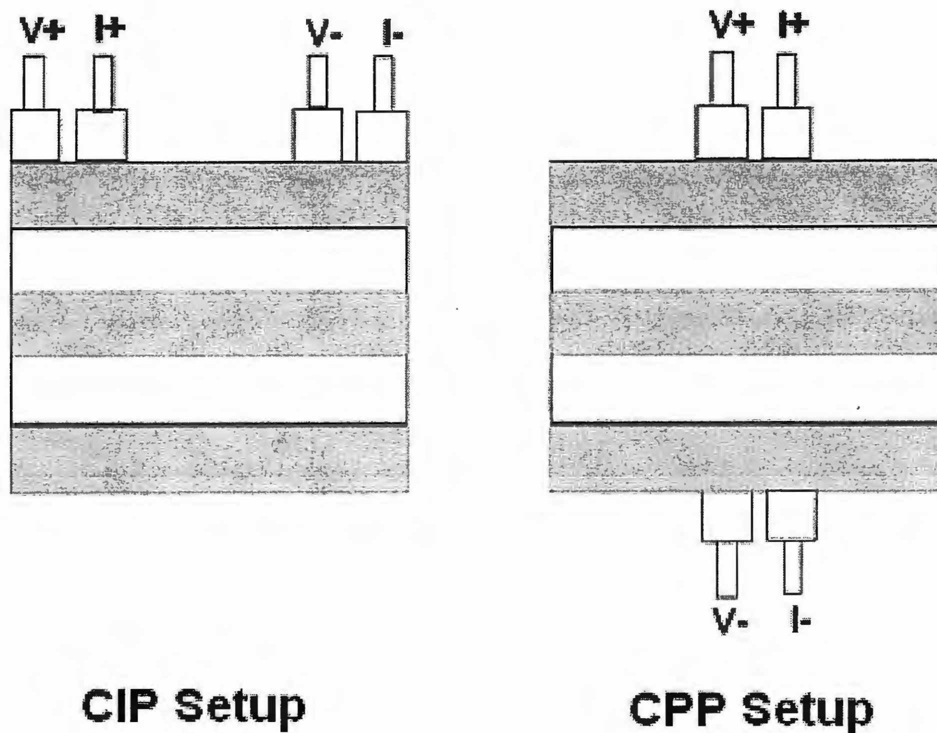

Figure 9 - CIP and CPP measurement setups

Experimental

This research project was broken into three stages. The first phase consisted of studying the field of GMR and selecting the type of GMR structure to pursue. The second stage was spent developing an understanding of the equipment and materials used, and designing a fabrication process. In the final stage, GMR devices were fabricated and characterized using a number of different tests.

Structure Description

The sandwich structure chosen was a modification of the simple ferromagnetic - nonmagnetic - ferromagnetic structure as proposed by Pohm at al [12]. The structure used in this project is shown below in Figure 10.

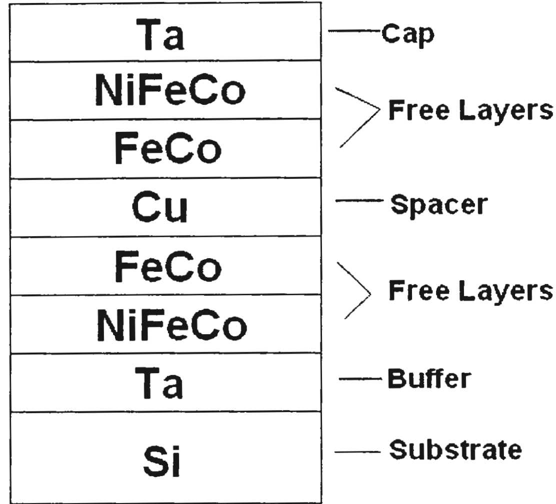

Figure 10 - GMR Sandwich Structure

The sandwich structure was deposited on a three inch Silicon (Si) wafer with an oxide layer of approximately 2000Å. Tantalum (Ta) was used as a seed layer at the base of the structure to promote smooth layer growth for the subsequent layers. The ferromagnetic layer was divided into two separate alloys. The first ferromagnetic alloy consisted of a ratio of 65% Ni 20% Fe 15% Co. The second ferromagnetic material was a 90% Co 10% Fe alloy. A Cu spacer layer was used to magnetically separate the ferromagnetic layers, allowing them to align independently of each other. The structure was then repeated in reverse, with the CoFe

المنارة للاستشارات
www.manaraa.com

layer and the NiFeCo layer following the spacer layer. The entire structure was topped with a thick Ta layer that helped protect the top ferromagnetic layer from oxidation.

Calibration of Evaporator

In GMR structures, the thickness and smoothness of the layers are very important. The Electron Beam (E-beam) Evaporator uses a crystal monitor to track the rate of deposition and film thickness. The crystal monitor utilizes the density and acoustic impedance of the material being deposited to perform its calculations. The accuracy of the crystal monitor is also determined by the geometry of the deposition chamber. Since it is impossible for the crystal monitor to be located at the surface of the wafer, an error must be accounted for based on the location of the monitor in reference to the metal source and the wafer surface. The percentage difference between the thickness measured by the crystal monitor and the thickness actually deposited on the substrate is called the tooling factor, and can be determined empirically. To find the tooling factor, a layer of material is deposited and the thickness reading on the monitor compared to the actual thickness as determined through other measurement techniques. The equation relating these values to the tooling is as follows:

$$Tooling(\%) = 100 * \frac{T_S}{T_X}$$

Where T_S is the actual thickness at the substrate and T_X is the thickness reading on the monitor.

المنارة للاستشارات
www.manaraa.com

Aluminum (Al) was deposited on Si substrates until the monitor showed 5000Å of metal. The Al was patterned and etched into strips using photoresist and ultra violet light exposure. The thickness was measured using a profilometer, which measures the changes in the surface of the film by allowing a small point to run across the surface. After adjusting the tooling, another film of Al was deposited and measured. This process was repeated until the thickness measured by the profilometer was within approximately 10% of the thickness displayed by the crystal monitor. The calibration was checked periodically by deposition of 1000Å Cu layers.

Mixing Metals

To allow for compositions of the ferromagnetic metals in the alloys to be varied, powdered metals were used. The desired composition was determined based on the weight of each metal, which was appropriate because the densities of the metals were fairly close. The metals were added directly to crucibles and mixed thoroughly with each other.

In order to use the crystal monitor to track the rate and thickness of deposition, the acoustic impedance and density of the materials were required. These values were tabulated in an Inficon 6000 technical manual for bulk materials, but could only be estimated for the alloy compositions. It was decided to use simple weighted averages of the composition materials to approximate the values. The estimated density and acoustic impedance of the alloys and the true values of the bulk materials are shown in Table 1.

المنارة للاستشارات

www.manaraa.com

Table 1 - Material density and acoustic impedance

Material	Density (g/cm^3)	Acoustic Impedance
Co	8.71	0.343
Fe	7.86	0.349
Ni	8.91	0.331
NiFeCo	8.74	0.336
FeCo	8.49	0.345

Evaporation

Deposition was done using a Temescal E-beam evaporation system. The system consists of a 10kV power supply used to generate an electron beam. The beam is a standard 270° arc focused by a permanent magnet [5]. A set of electromagnets allows the E-Beam to be positioned and swept across the metal for a controlled and even melting. The pressure of the system during deposition is normally on the order of 10^{-8} Torr, which should be sufficient to prevent oxidation of the film during growth. The deposition is controlled by an Inficon 6000 control system, which allows for complete programming of the deposition process and monitors the rate and thickness of the deposition.

The use of unknown metals and powdered alloys required special attention to thoroughly test the evaporation process. The evaporation of Ta shots worked well, but required a very narrow focus of the E-beam to achieve sufficient deposition rates. The alloys on the other hand, presented a very large obstacle.

المنارة للاستشارات
www.manaraa.com

Prior to evaporation, the powdered metals required a great deal of preheating to fully outgas any trapped oxygen. Initially, the alloys were evaporated in graphite crucibles. During the evaporation process, both the NiFeCo and FeCo alloys spit metal severely. Regardless of the heating ramp and sweep of the E-beam, the alloys remained highly unstable. In an attempt to remedy the problem, Alumina crucibles were used for evaporation of the alloys. Because of Alumina's excellent insulating properties, Ta wires were initially used to create a path for the electrons to flow to ground. Unfortunately, the heating of the Ta wires resulted in the cracking of the crucibles, and there was concern that the Ta may contaminate the alloys. It was determined that the cracks allowed a path for electron flow without the use of Ta wires, so the wires were removed. Using the Alumina crucibles allowed for a slow deposition rate, but spitting still occurred if the deposition was not closely monitored. The cracks in the Alumina crucibles were later believed to cause contamination, so the alloys were returned to graphite crucibles, but no change in contamination was found.

The cause of the severe spitting is believed to have come from oxygen residing on the large porous surface of the powdered metals. The powdered metals were later replaced with 0.125 shot bulk metals, which allowed higher deposition rates without spitting.

Magnetic Field Generation

In order to induce magnetic anisotropy within the magnetic layers, it is necessary to deposit the ferromagnetic materials in a magnetic field. To achieve a uniform magnetic field across the surface of the wafer, a set of Helmholtz coils [8] was designed, constructed, and

المنارة للاستشارات
www.manaraa.com

used. Helmholtz coils consist of a pair of wire coils separated by a distance equal to the coil radius, thus creating a uniform unidirectional magnetic field within the evaporation chamber.

The magnetic field generated by a coil of N turns of wire can be approximated using the equation [8]:

$$B(z) = \frac{\mu_0 I N r^2}{2(r^2 + x^2)^{3/2}}$$

Where r is the radius of the coil, N is the number of turns, I is the current through the wire, x is the distance from the center of the coil and μ_0 is the permeability of air. If two coils are placed a distance a apart and x is measured from the center point between the two coils, the formula for the magnetic field becomes [8]:

$$B(z) = \frac{\mu_0 I N r^2}{2}\left[\frac{1}{(r^2 + \left(x + \frac{a}{2}\right)^2)^{3/2}} + \frac{1}{(r^2 + \left(x - \frac{a}{2}\right)^2)^{3/2}}\right]$$

The placement of the Helmholtz coils inside the evaporation system was considered, but the requirements for cooling in the vacuum made it impractical. It was ultimately decided to mount the coils externally on the E-beam system. This choice imposed strict design requirements on the coils, as there was limited space for the coils to fit. The final coils had a radius of 16 inches and were separated by 15 inches with 80 turns per coil. The measured field for 30 Amps operation was found to be 49 Gauss, which is sufficient to align the magnetic axis and induce anisotropy within the materials.

المنارة للاستشارات

www.manaraa.com

Fabrication Process

The first step in the fabrication process was to thoroughly clean the Si substrates. The substrates were cleansed in a solution of 2500mL DI H_2O + 500mL NH_4OH + 400mL H_2O_2 for 15 minutes at 80° C. They were rinsed in DI water and dipped in a 50:1 HF acid solution. A second soak in 3000mL DI H_2O + 500 mL HCl + 500mL H_2O_2 completed the cleaning process. This standard cleaning process ensured that most contaminates including any oxidation on the substrate were removed.

A layer of oxide was then grown on the wafers using an oxidation furnace. The desired thickness of oxide ranged from 1500Å to 2500Å. Using standard lithography techniques, the wafers were patterned with photoresist to prepare for lift off. The wafers were loaded into the evaporator, allowing the pressure to return to the low 10^{-8} Torr range. Table 2 shows the deposition rate, percent power, and thickness range for each individual layer.

Table 2 - Fabrication Process

Layer	Metal	Deposition Rate	Thickness Range
1	Ta	1Å/s @ 14%	50Å
2	Ni Fe Co	0.1-0.2Å/s @ 12%	40-60Å
3	Fe Co	0.2-0.3Å/s @ 12%	10-30Å
4	Cu	1Å/s @ 12%	20-40Å
5	Fe Co	0.2-0.3Å/s @ 12%	10-30Å
6	Ni Fe Co	0.1-0.2Å/s	40-80Å
7	Ta	1Å/s @ 14%	100-200Å

المنارة للاستشارات
www.manaraa.com

The thicknesses of the layers were varied on different samples in an attempt to improve GMR effects.

After the fabrication of the GMR structure, the wafers were placed in an acetone bath to lift off and pattern the devices. The wafer was then thoroughly rinsed and dried with nitrogen. Some wafers were annealed at 285°C in a magnetic field of approximately 20 Gauss, to improve anisotropy. Individual devices were cut apart using a diamond scribe. Test structures that required contacts had Indium foil pressed on and heated.

Characterization

Profilometry

Profilometry measurements were taken to check the calibration of the E-beam evaporation system. The system utilizes a needle lightly pressed on the surface of the sample. As the needle is run across the surface of the sample, the pressure applied to the needle is tracked. A change in pressure indicates a difference in thickness along the surface of the substrate. The profilometer interprets the pressure data into depth change and plots the surface profile of the sample. By patterning a row of bars across the sample surface, it is possible to measure its approximate thickness.

Two different profilometers were used throughout this project. The first was an older system that used a separate plotter to output the data. This profilometer outputs the height information in the form of a voltage signal. The plotter printed the voltage signal to show the profile of the wafer surface, but did not make any calculation for layer thickness. To obtain

المنارة للاستشارات
www.manaraa.com

layer thickness, the length of the plotted line was measured by hand and multiplied by a scalar value determined by the settings of the profilometer. A major drawback of this system is the error associated with hand measurements of lines. The second profilometry system used was a newer automatic system. The sample was placed onto the profilometer and was leveled. Using a computerized interface, the sweep of the needle was set. The computer controlled the measurement process, calculated, and printed out a surface profile and layer thickness.

Four Point Probe

In order to find the resistivity of the deposited layers, a linear four point probe configuration with a space of 0.1016 cm between the probe tips was used. An input current was supplied through the outer two probes, and the resulting voltage was measured between the two inner probes.

Voltage was measured at five current values ranging from 5 mA to 25 mA in five different areas of the wafer. The measured voltage was divided by the input current to calculate the resistance of the layer. These resistances were used in subsequent calculations. To account for thin film effects, the correction factor (F) was found using the following equation:

$$F = \frac{t}{2s} \ln\left(\frac{\sinh\left(t/s \right)}{\sinh\left(t/2s \right)} \right)^{-1}$$

المنارة للاستشارات
www.manaraa.com

Where t is the thickness of the layer and s is the probe spacing. For films where the layer thickness was much smaller than the probe spacing, the correction factor equation was simplified, because the hyperbolic sign portions simply reduce to two:

$$F = \frac{t}{2s} \ln(2)^{-1}$$

The resistivity was easy to find with the following equation:

$$\rho = (2\pi) sRF$$

Where R is the average resistance of the sample in one area. Another useful property of the layers was the sheet resistance, determined by dividing the resistivity by the film thickness.

$$R_S = \frac{\rho}{t}$$

GMR Measurements

The samples were prepared for testing using three unique methods to measure for GMR effects. Early project tests utilized whole wafers or small squares of the sample. Later, the structures were patterned in two different ways in attempts to improve detection of GMR.

Bulk Sample

Initially, it was believed that the GMR could be measured in the bulk wafer using only the four point probe system. The change in output voltage was measured as a magnetic field was applied. It was later found that the linear configuration of the four point probe was

المنارة للاستشارات
www.manaraa.com

not conducive for the needed measurements. Instead a rectangular four point probe measurement was needed.

The samples were broken into smaller devices on the order of 1 cm^2. Contact to a sample was made at each of the four corners using four small clips of metal mounted on a Plexiglas border. Wires ran from the metal clips to output triaxial connections. The resistance was tracked using an Hewlett Packard 4145 semiconductor test station. A source current was applied to two adjacent corners, and the generated voltage was measured across the other corners. A magnetic field was generated both by a large electromagnet capable of 5000Oe and a permanent magnet. Many variations of these measurements were carried out with the shape of the sample ranging from square to rectangle.

The mounting of the samples became difficult as smaller sizes were tested. An attempt was made to use a semiconductor test station with small probe needles, but it proved too difficult to introduce a magnetic field during tests due to the limited amount of space in the mounting area. This approach was abandoned in favor of etched samples.

Van der Paw

The GMR samples were patterned into Van der Paw patterns [15] using lift off techniques. Two different Van der Paw patterns were used and are shown in Figure 11.

المنارة للاستشارات

www.manaraa.com

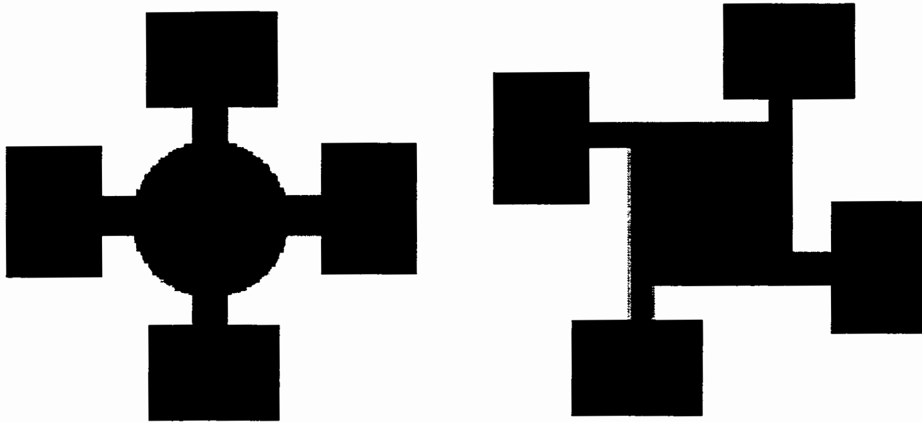

Figure 11 - Van der Paw Test Patterns

Contact to both Van der Paw patterns was made at the large rectangular contact areas at the end of the bars. An ohmic contact was made with the GMR structure through the use of Indium foil. Small squares of the foil were adhered to the structure using direct pressure, and the sample was heated to ensure good contact. One mil gold wire was then pressed lightly into the Indium contact with the other end soldered to a large copper contact interface. A source current was applied at the copper contact to two of the bars, and the resulting voltage was measured across the other two bars.

The Van der Paw pattern to the left was used first and had an inner area of 2 mm. It was suggested that smaller test areas might show more pronounced GMR effects, so a new mask with the Van der Paw pattern on the right was created. The inner square of the new Van der Paw patterns range from 10 μm to 2 mm.

Bar Resistors

Pohm et al. have found that the use of bar resistors, as shown in Figure 12, allow for better detection of GMR effects [12].

Figure 12 - Bar resistor

Magnetic fields generated by each ferromagnetic layer arise along the width of the bar in opposition to each other, causing the ferromagnetic layers to favor an antiparallel alignment.

The bar resistors were also patterned using the lift off process. Contact to the sample was again made using Indium foil. A multimeter was used to sense resistance across the two contacts. This resistance was monitored as a magnetic field was applied.

The sheet resistance of the film can also be found using a bar magnet if the width and length of the bar is known. The sheet resistance is calculated by dividing the measured resistance by the ratio of length to width of the bar.

Scanning Electron Microscopy

Scanning Electron Microscopy (SEM) analysis allows for the surface of a sample to be examined at very high magnification with high resolution. The SEM often allows for a resolution of 4nm, a magnification of tens of thousand, and a very large depth-of-field enabling the viewing of samples in three-dimensions. These features allow for the examination of surface continuity, defects, and interfaces.

The SEM uses an Electron Beam Gun to generate and accelerate electrons towards the sample. The E-beam source is designed to focus the emitted electrons into a small beam so they can be approximated as a point source; this is important for mathematically constructing a final image. To help achieve a clear image, the emitted electrons must all have similar energy levels. Finally, the electrons must travel on a path that is straight towards the sample. After exiting the gun, the electrons pass through a series of coils that control the beam energy, filter out any high-angle electrons, and focus remaining electrons into a tighter beam. The electron beam scans across the surface of the sample, pausing every few microseconds to gather information. As the electron beam strikes the sample surface, a number of interactions occur.

Backscattered electrons

When an electron interacts with an atom in the sample, it is reflected away from the sample and is known as a backscattered electron. The angle at which the electron is reflected is dependent on the orientation of the atom in the structure, but normally the backscattered electrons are reflected nearly 180° from their incoming path. The amount of backscattered

المنارة للاستشارات
www.manaraa.com

electrons is determined by the atomic number of the struck atom, with higher numbers causing more backscattering. The number of backscattered electrons are collected and used to create an image of the surface structure.

Secondary Electrons

The second interaction arises in the form of secondary electrons. As an electron passes near an atom in the structure, it can pass some of its energy to lower energy electrons in orbit around the atom. This additional energy allows electrons close to the surface of the sample to leave the atom. Secondary electrons are collected independently of the backscattered electrons and amplified because of their low energy levels. The production of secondary electrons is strongly dependent on the surface structure of the sample, and is used to acquire detailed topographical images.

X-Ray Diffraction

The creation of a secondary electron results in a vacancy in a low energy shell of an atom. A higher energy electron can fall into the lower energy state, but must give off any extra energy to balance the total energy of the atom. This extra energy is usually emitted in the form of X-rays and is the basis of the X-ray diffraction measurements. The X-rays generated have a unique energy level based on what type of atom from which they come. These energy levels can be monitored and sorted giving the composition of the sample.

المنارة للاستشارات
www.manaraa.com

Results and Discussion

GMR films were deposited on Si wafers following the fabrication procedure previously described. In total, 30 different sandwich structures were fabricated and tested. The parameters for each structure are listed in Table 3.

Table 3 - GMR Sandwich Structure Growth Parameters

Sample ID	T_{ox}	T_1	T_2	T_3	T_4	T_5	T_6	T_7	Annealed	Test
0800-01	2000	40	40	13	27	13	40	85		1
0800-02	2000	40	40	13	27	13	40	85		1
0701-01	0	40	40	15	29	15	40	80		1
0801-01	2000	40	40	15	27	15	40	100		1
0801-02	2500	40	40	12	25	12	40	100		1
0801-03	2500	40	40	12	25	12	40 *	100		2
0801-04	2500	40	45	15	28	15	55	100		2
0901-01	2500	40	45	15	28	15	55 *	100		2
0901-02	0	40	45	15	28	15	55 *	100		2
0901-03	0	50	40	15	27	15	60*	100		2
1001-01	2000	40	40	15	20	15 *	55 *	100	Yes	3
1001-02	2000	40	40	15	25	15 *	55 *	100	Yes	3
1101-01	2000	40	40	15	30	15 *	55 *	100	Yes	3
1101-02	2000	40	40	15	35	15 *	55 *	100	Yes	3
0202-01	0	40	40	15	20	15 *	55 *	100	Yes	3
0202-02	0	40	40	15	25	15 *	55 *	100	Yes	3-4
0302-01	0	40	40	15	30	15 *	55 *	100	Yes	3-4
0302-02	0	40	40	15	35	15 *	55 *	100	Yes	3-4
0302-03	1600	50	40 *	15 *	32	15 *	40 *	100	Yes	3-4
0402-01	1600	50	40 *	15 *	30	15 *	60 *	100	Yes	4
0402-02	1600	50	40 *	15 *	30	15 *	40 *	100	Yes	4

المنارة للاستشارات
www.manaraa.com

Table 3 - GMR Sandwich Structure Growth Parameters Cont.

Sample ID	T_{ox}	T_1	T_2	T_3	T_4	T_5	T_6	T_7	Annealed	Test
0402-03	1600	50	50 *	19 *	38	19 *	50 *	100	Yes	4
0502-01	1600	50	40 *	15 *	30	15 *	40 *	100	Yes	4
0502-02	1600	50	0	40 *	30	40 *	0	100	Yes	4
0502-03	1600	50	0	40 *	30	50 *	0	100	Yes	4
0502-04	1600	50	40 *	15 *	35	15 *	40 *	100	Yes	4
0602-01	1600	50	40 *	15 *	30	15 *	40 *	100	Yes	4
0602-02	1600	50	40 *	15 *	25	15 *	40 *	100	Yes	4
0602-03	1600	50	40 *	0	30	0	40 *	100	Yes	4
0702-01	1600	50	0	40 *	30	40 *	0	100	Yes	4

* - Denotes layers deposited within a magnetic field

The thicknesses listed in Table 3 correspond to those shown in Figure 13.

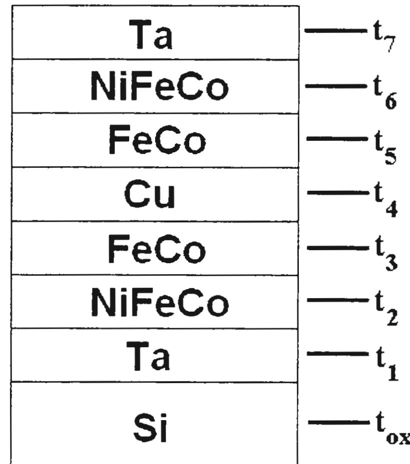

Figure 13 - GMR Sandwich Structure

In addition to the ferromagnetic/non-magnetic/ferromagnetic structures that were fabricated, two other types of devices were attempted. First, four samples of alternating Fe

المنارة للاستشارات
www.manaraa.com

and Co layers repeated five, ten, fifteen, and twenty times respectively were fabricated.

Secondly, a spin-valve with a pinned layer as shown in Figure 14 was fabricated.

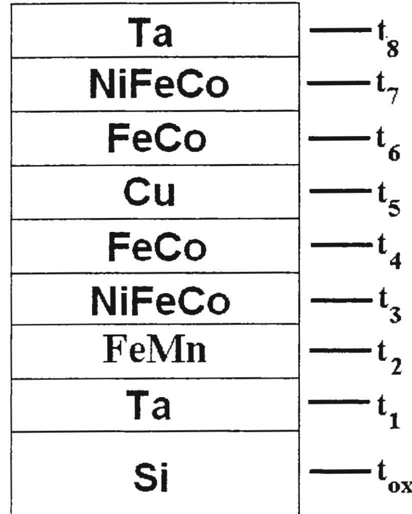

Figure 14 -GMR Spin-Valve Structure

Table 4 lists the parameters for the spin-valve structure in Figure 14.

Table 4 - GMR Spin-valve Structure Growth Parameters

Sample ID	T_{ox}	T_1	T_2	T_3	T_4	T_5	T_6	T_7	T_8
0202-SV1	0	45	75	35	15	25	15	35	45
0202-SV2	2000	45	75	35	15	25	15	35	45
0202-SV3	1600	50	40	40	15	30	15	40	100

GMR Measurements

The samples listed in Table 3 had varying tests performed on them, as noted in the 'Test' column. Early samples were tested using a linear four-point probe setup and are

المنارة للاستشارات
www.manaraa.com

denoted by a '1' in the 'Test' column. After discovering that a linear four-point probe test would not show GMR effects, the samples were cut into small squares, contact was made to each of the four corners, and voltage-current measurements were taken. A '2' in the test column indicate samples tested using this method. Tests marked '3' and '4' utilized a photoresist liftoff, allowing for smaller devices to be tested. Tests of type '3' were performed on small Van der Paw shapes, using an input current and measuring the output voltage. The test '4' patterns were simple bar resistors with two contacts.

Each sample was tested in multiple locations across the wafer. Type '2' tests were performed on varying sizes of squares and rectangles for each sample. Type '3' and '4' tests were performed on at least five different sizes of devices. None of the tests yielded meaningful levels of resistance changes, each test yielding less than 0.2% change. The testing procedure was verified through the use of known working samples acquired from an independent source and was found to be accurate to the expected results. The test samples were further characterized in an attempt to discern what was preventing them from showing GMR effects.

Hysteresis Measurements

To gain an idea of what was happening magnetically within the samples, hysteresis measurements were performed on two different samples. Hysteresis measurements test the magnetic characteristics of an entire wafer by applying a magnetic field and measuring the magnetization that arises.

المنارة للاستشارات

www.manaraa.com

The first wafer tested had the same thickness and structure as sample 0302-03 in Table 3. The magnetic field vs. flux plot can be seen in Figure 15.

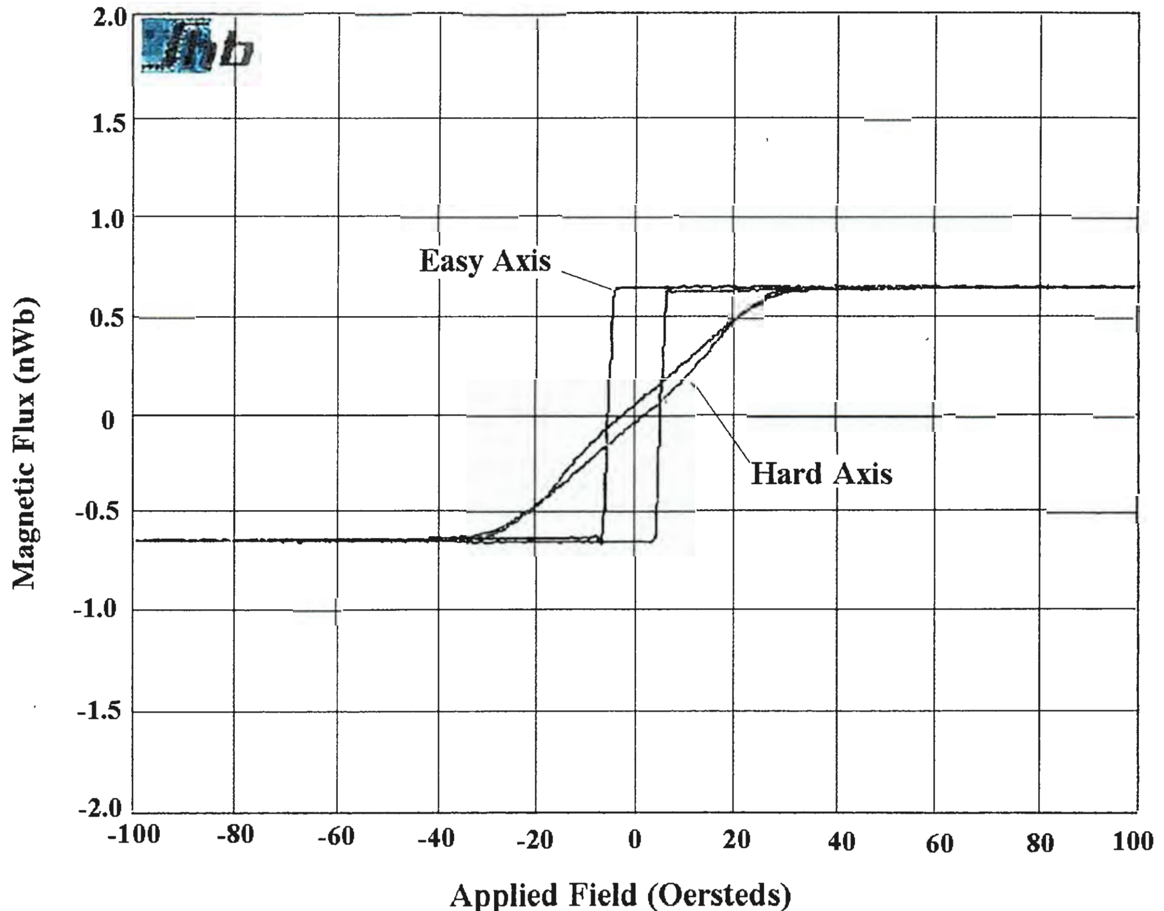

Figure 15 - Hysteresis plot 1

Looking at the hysteresis in Figure 15, it is seen that the easy and hard axes of the structure react differently from each other, also know as anisotropy. The easy axis has sharp transitions from low to high magnetization as the applied field changes. The transition of the easy axis occurs at 5.4 Oe. The hard layer's magnetization switches more gradual between -40 Oe to 35 Oe. The saturation magnetization of both axes is 0.65 nWb and the coercivity point is at 2.28 Oe. A closer examination of the easy axis reveals that the two ferromagnetic

المنارة للاستشارات
www.manaraa.com

layers switch magnetization direction at nearly the same fields. Although this is normal for samples of this type and thickness, it is highly possible that any GMR effects would be missed without extremely fine control over the applied field.

The second sample tested had the same thickness and layers as sample 0402-01 in Table 3. This sample had a different thickness for each of the NiFeCo layers. This difference was added in hopes of increasing the separation in switching fields between the two ferromagnetic layers. The hysteresis for this sample is shown in Figure 16.

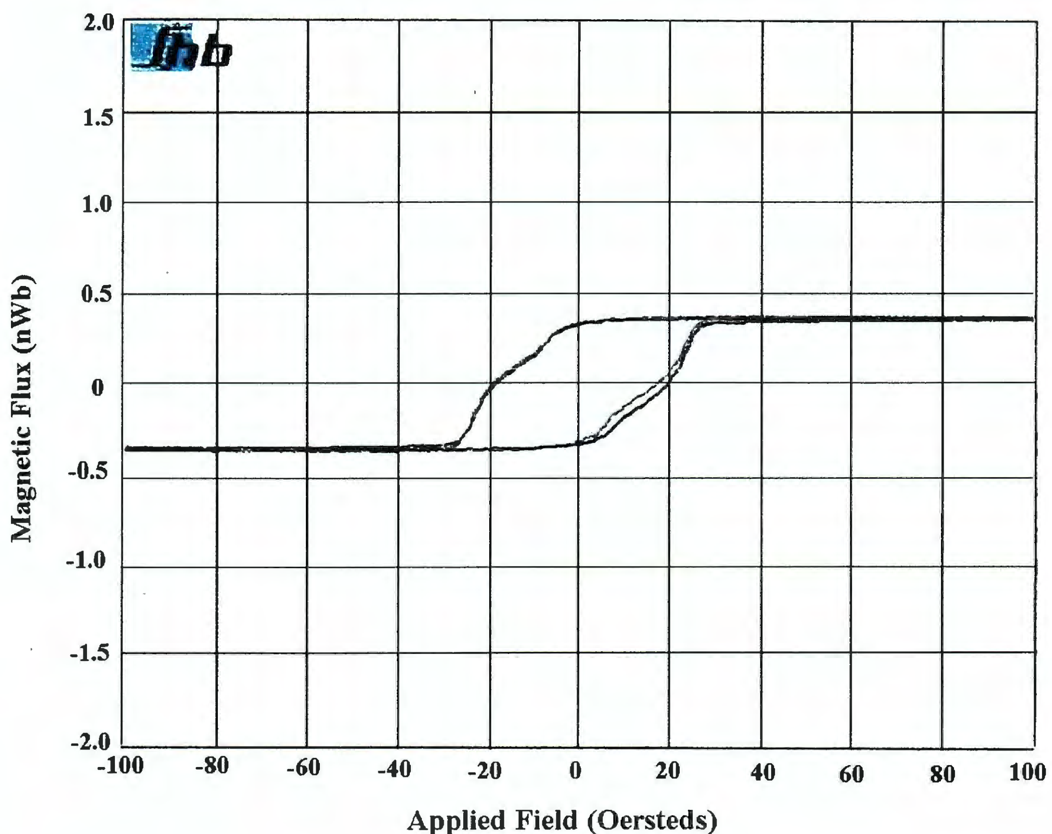

Figure 16 - Hysteresis plot 2

The ferromagnetic layers are seen to switch independently from each other, at 5 Oe and 10 Oe respectively. However, both the easy and hard axes react to the applied field in the same way, meaning the anisotropy seen in the first sample was lost. This may be the result of insufficient magnetic field during fabrication. A 300° annealing in a 50 Oe magnetic field was unable to induce anisotropy.

Resistivity and Sheet Resistance

Using linear four-point probe measurements, many GMR stacks and single layer films were measured to find the resistivity and sheet resistance. The electrical resistivity of a single Cu layer was found to be close to the expected value for a bulk material, the small difference mainly due to thin film effects. Because of the good correlation, the Cu layers were believed to be relatively pure. Measurements on the GMR stacks revealed sheet resistances on the order of 157–191 ohms per square. These were much higher than the 10-20 ohms per square that was expected. The high sheet resistance of the devices indicated that there may have been a significant amount of oxygen within some of the layers. Very little information could be gathered from resistivity measurements of single alloy films because the resistivity of the bulk alloy composition was not exact and could only be predicted. To further investigate the contamination of the layers, a different characterization was needed.

www.manaraa.com

X-Ray Diffraction

Oxygen Incorporation

Through the use of X-ray diffraction (XRD), the composition of individual layers was determined. The first sample analyzed using XRD was a 1000Å thick layer of the NiFeCo alloy grown on a SiO_2 layer. The composition analysis of the sample is shown in Figure 17.

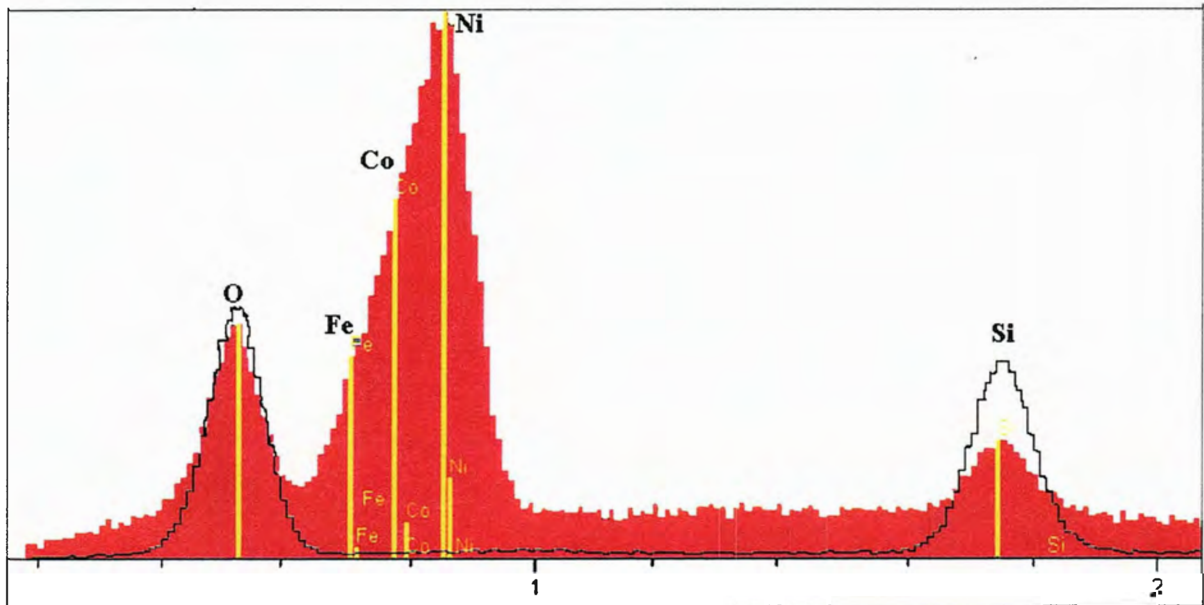

Figure 17 - NiFeCo Composition Plot (Powdered Metals)

Figure 17 shows a plot of both the NiFeCo layer and the Silicon dioxide (SiO_2) layer. The NiFeCo layer is displayed as the solid bars and the SiO_2 is the lined outline. Comparing the two layers, the level of Si dropped in intensity while the oxygen (O_2) level remained constant. This indicated that there was a significant amount of O_2 in the NiFeCo alloy layer. In an attempt to remedy this problem, the powdered metals were replaced with metals in a

www.manaraa.com

larger shot form. The powdered metals were believed to be more porous with a larger surface area, allowing for a great deal of oxygen contamination.

A second 1000Å thick sample of NiFeCo was grown on a SiO_2 layer and analyzed using XRD. Figure 18 shows a comparison between the NiFeCo alloy layer and the SiO_2 layer of this sample. As with the previous sample, the amount of Si present drops off between the two layers, but the O_2 content remains the same.

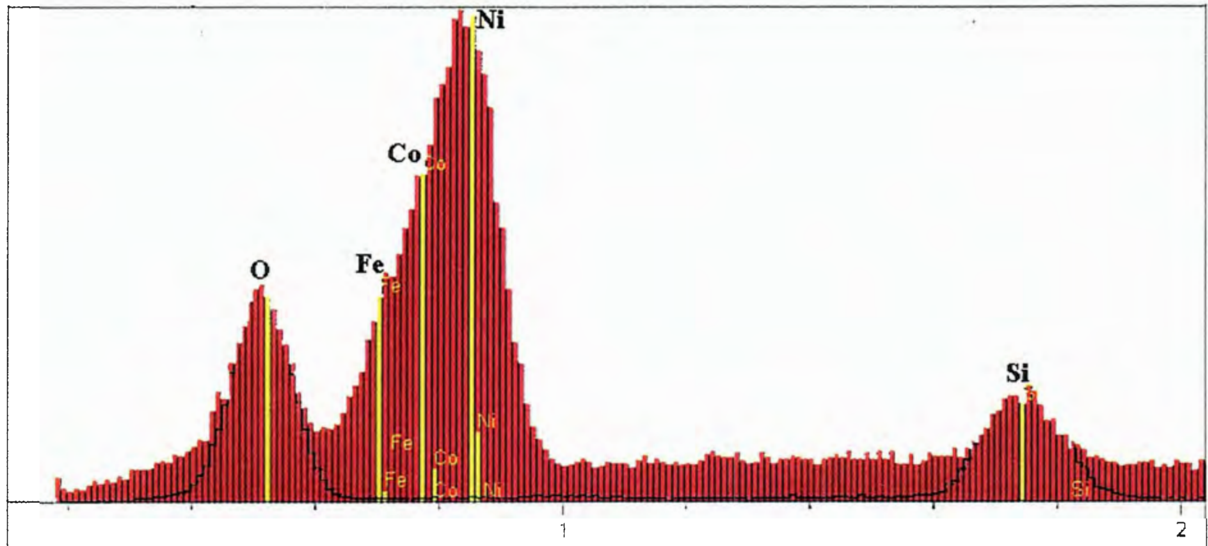

Figure 18 - NiFeCo Composition Plot (Shot Metals)

This showed that the O_2 found in the two samples was independent of the form of metal used during deposition. The deposition chamber was kept at a low pressure in the range of the lower 10^{-7} Torr, so there was little concern that O_2 was introduced into the layers during the evaporation process. Further analysis of the data suggested that the O_2 seen in the XRD analysis was most likely due to X-rays leaking through the NiFeCo layer from the SiO_2 layer.

المنارة للاستشارات
www.manaraa.com

Layer Composition

Although the alloys were mixed as precisely as possible, there was always concern that different melting temperatures and vapor pressures of the individual metals might cause the alloy deposited on the wafer to differ significantly from the desired alloy in the crucible. In addition to investigating the occurrence of O_2 in the samples, the XRD analysis allowed a look at the composition of the alloy at the surface of the wafer. In Figures 17 and 18, the composition of the alloys was estimated by looking at the relative heights of the three metals, a good first order approximation. Measuring the two plots yielded a similar composition estimate of 59% Ni 19% Fe 22% Co, which was close enough to the desired 65% Ni 15% Fe 20% Co to work in the fabricated structure.

Discussion

A number of possible problem areas were identified and worked on, yet improvements were few and far between. A precise balance of variables and processes occurring within the layers is necessary to show GMR effects. There are many possibilities of what may have caused the lack of GMR effects in the fabricated samples.

First, the uniformity of layer thickness across the surface of the wafer is very important. The deposition system was believed to be capable of producing the necessary uniform films, but with such thin layers it became difficult to predict the final product. The alloy compositions had a tendency to spit during evaporation, resulting in non-uniformity or uneven layers. Further investigation of these possibilities would require the use of an

المنارة للاستشارات
www.manaraa.com

advanced profilometry system capable of tracking minute changes across the surface of the wafer.

Next, the interface between layers is very important. Any defects at the interfaces will cause the mean-free path of the electrons to be greatly reduced, increasing the resistance of the device. The uniformity of the layers also plays an important role in the quality of the interface. Large thickness gradients increase the likeliness of defects between layers. Another possible interface problem may arise if there is sufficient oxygen in the system to oxidize layers between depositions. A third possible problem involves the intermixing between two adjacent layers during deposition. This is mostly a concern at the ferromagnetic/spacer interfaces. If the temperature of the wafer rises enough during deposition, the metal being deposited may be able to displace atoms of the previous layer resulting in a FeCoCu alloy at the interface. To investigate these possibilities, further SEM and XRD analysis is necessary. Samples two layers thick would need to be examined along the edge of the wafer, allowing for a look at the profile of the interface. Through use of the SEM, the surface of the interface could be viewed to determine the uniformity of the layers. Using XRD, the composition of the metal at the interface could be resolved. The amount and depth of mixing, if any, could also be determined.

A large drawback to doing characterization with the profilometry, SEM, and XRD tests is that they require layer thicknesses that are much greater than those used for the actual devices. The fact that the layer structure appears one way on a 1000Å sample does not necessarily mean they will be the same for a 40Å sample.

المنارة للاستشارات

www.manaraa.com

Conclusions

While this project was not completely successful in obtaining GMR effects, it did lay the ground work for future research into the subject. Significant research was done into the background of GMR, building a knowledge-base of information. A process was developed for the equipment available, and testing procedures were developed and verified. Helmholtz coils were installed around the deposition chamber to allow for fabrication in a magnetic field. Finally, the available equipment was brought into working order, calibrated, and configured for GMR fabrication.

Giant Magnetoresistant sandwich structures were deposited on Si substrates using E-beam evaporation. Many samples were fabricated while varying layer thickness in an effort to obtain GMR effects. The samples were tested using multiple techniques and test equipment. To rule out test station error, independently fabricated samples were used as controls to show GMR effects using the test equipment. Additional samples were tested to obtain hysteresis plots, resistivity and sheet resistance measurements, and composition information in attempts to determine why the fabricated samples did not show GMR effects.

Results from the hysteresis plots showed that the samples did react to an applied field as expected, indicating that they ought to show GMR. The two ferromagnetic layers were found to switch at very close fields, but should not have prevented GMR effects from being evident. Attempts to increase the difference in switching fields resulted in a loss of anisotropy. Saturation magnetization, coercivity, and switching field of the samples were within desired parameters.

المنارة للاستشارات
www.manaraa.com

Four-point probe measurements revealed higher than expected resistivity and sheet resistance. A possible cause of the increase could be contamination of the layers, but no such contaminant could be located using X-ray diffraction measurements. The oxygen found in the XRD measurements was believed to come from the oxide layer on the silicon, so was discounted as a contaminant. Finally, the composition of the layers was verified through the XRD measurements. A first order estimate of the composition showed that the alloy was within an acceptable range.

Testing procedures were developed for the research center with supplies and equipment on hand. A complete probe station with Helmholtz coils, current source, and voltage meter was assembled, although was determined impractical for the measurements of the devices fabricated. The use of a large electromagnet with small clip probes and indium/gold wire contacts was developed and proved reliable for testing independently grown samples. Photoresist liftoff techniques were shown to work on the GMR structures down to details of 4 μm. Finally, a photoresist image reversal process was tested and calibrated for use on available equipment.

المنارة للاستشارات

www.manaraa.com

References

[1] Baibich, M. N., Broto, J. M., Fert, A. *et al.* (1988) *Phys. Rev. Letts.,* **61**: 2472.

[2] Binash, G., Grunberg, P., Saurenbach, F. and Zinn, W. (1989) *Phys. Rev. B,* **39**: 4828.

[3] Department of Energy's Oak Ridge National Laboratory website; available from *http://www.ornl.gov/*; internet; accessed on November 2001.

[4] Dieny, B., (1994) *J. Magn. Magn. Mater.*, **136**: 335.

[5] Glocker, David A., Shah, S. Ismat (1995) Handbook of Thin Film Process Technology. Philadelphia; Institute of Physics.

[6] Dieny, B., Speriosu, V. S., Parkin, S. S. P., Gumey, B. A., Wilhoit, D.R., and Mauri, D., (1991) *Phys. Rev. B,* **43**, 1297.

[7] McCord, J., Hubert, A. (1997) *IEEE Trans. Magnetics*, V.33, No. 5: 3984.

[8] Monsma, D. J., Lodder, J. C., Dieny, B. and Popma, Th. J. A (1995) *Phys. Rev. Letts.,* **74**: 5260.

[9] O'Neill, Daniel (2001) *Mathematical Modeling of the Magnetic Field of a Helmholtz Coil* [on-line] Bloomington, IN: Indiana University; available from http://dustbunny.physics.indiana.edu/~dzierba/iustatus/HC_don.pdf; internet; accessed on February 8, 2001.

[10] Pierret, Robert F., Advanced Semiconductor Fundamentals, Massachesetts: Addison-Wesley Publiching Company, 1989.

[11] Pohm, A., Cornstock, C. and Hurst, A. (1990) *J. Appl. Phys.,* **67:** 4881.

المنارة للاستشارات

www.manaraa.com

[12] Pohm, A. V., Everitt, B. A., Beech, R. S., Daughton, J. M. (1997) *IEEE Trans. Magnetics,* **33**: 3280.

[13] Pohm, A. V.; Professor Emeritus Department of Computer and Electrical Engineering, Iowa State University, (2000-2002) Private communications.

[14] Ripka, M. Tondra, J. Stokes, and R. Beech (1999) *Sensors and Actuators A,* Vol. 76: 227-232.

[15] Trout, S. R. (1988) *IEEE Trans Magnetics*, V.24, No. 4: 2108.

[16] Van der Paw, L. J. (1958) *Phillips Research Reports,* 19: 1-9.

[17] White, Robert L. (1992) *IEEE Trans. Magnetics,* V.28, No. 5: 2482.

المنارة للاستشارات

www.manaraa.com

Acknowledgements

I would like to use this opportunity to thank those who were instrumental in my graduate career.

First, I would like to thank my major professor Dr. Gary Tuttle for the opportunity to pursue this graduate work. His guidance and patients throughout this project proved invaluable to my development. My thanks go out to my committee members Dr. Vikram Dalal and Dr. Alan Constant for their support in finishing my research and thesis. I would also like to thank Dr. Arthur Pohm for countless morning meetings in attempt to find the cause of all our problems.

Thank you, to Qi Chen, Micah Decker, Tom Lloyd, Curtis Sell, Tris and Rius Tanadi, and Jon Williams for being there to talk, laugh, vent and otherwise help me keep my sanity.

My family deserves many thanks for their continuous love and support throughout these years of hard work.

Finally, I must thank my wife Cara Lea, for her endless support and encouragement throughout my research, and being with me when I needed her the most.

المنارة للاستشارات
www.manaraa.com